Highly Sensitive OFET Based Room Temperature Operated Gas Sensors Using Thieno[3,2-b]thiophene Extended Phthalocyanine Semiconductor

DOI:
10.1039/D4TC03208J

Document Version
Accepted author manuscript

Published in:
Journal of Materials Chemistry C

Journal of
Materials Chemistry C

Materials for optical, magnetic and electronic devices

Accepted Manuscript

This article can be cited before page numbers have been issued, to do this please use: T. Ozturk, R. Isci, O. Yavuz, S. Faraji, D. Gunturkun, M. S. Eroglu, L. A. Majewski and I. Yilmaz, *J. Mater. Chem. C*, 2024, DOI: 10.1039/D4TC03208J.

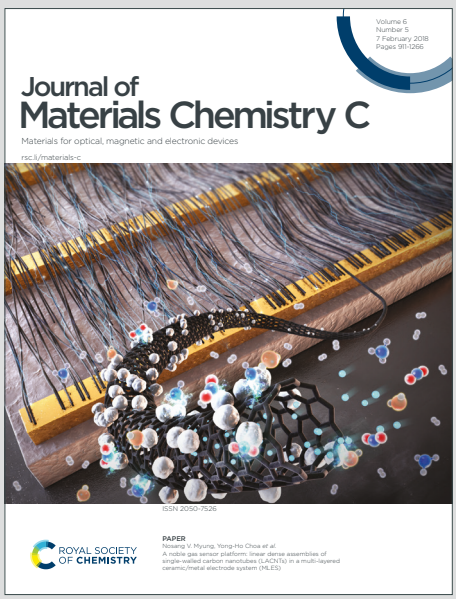

ROYAL SOCIETY OF CHEMISTRY

rsc.li/materials-c

Highly Sensitive OFET Based Room Temperature Operated Gas Sensors Using Thieno[3,2-*b*]thiophene Extended Phthalocyanine Semiconductor

Recep Isci[1,*], Ozgur Yavuz[1], Sheida Faraji[1,2], Dilara Gunturkun[1], Mehmet Eroglu[3,4], Leszek A. Majewski[2], Ismail Yilmaz[1,*] and Turan Ozturk[1,3,*]

[1]Istanbul Technical University, Chemistry Department, 34469, Maslak, Istanbul, Turkey.

[2]Department of Electrical and Electronic Engineering, University of Manchester, Engineering Building A, Oxford Road, Manchester M13 9PL, Manchester M13 9PL, UK.

[3]TUBITAK UME, Chemistry Group Laboratories, 41470, Gebze, Kocaeli, Turkey.

[4]Metallurgical and Materials Engineering Dept., Faculty of Engineering, Marmara University, Aydınevler, Maltepe, 34854, Istanbul, Turkey.

Abstract

Over the past decades, organic field-effect transistor (OFET) gas sensors have maintained a rapid development. However, the majority of OFET gas sensors show insufficient detection capability towards oxidizing and hazardous gases such as nitrogen dioxide (NO_2) and sulfide dioxide (SO_2). In this report, a sustainable approach toward fabrication of OFET gas sensor, consisting of thieno[3,2-*b*]thiophene (TT) and phthalocyanine (Pc) based electron rich structure (**TT-Pc**) for detection of both nitrogen dioxide (NO_2) and sulfide dioxide (SO_2) is disclosed for the first time. Khaya gum (KG), a natural, biodegradable biopolymer is used as the gate dielectric in these OFET-based sensors. Thin film properties and surface morphology of **TT-Pc** were investigated by UV-Vis, SEM, AFM and contact angle measurements, which indicated a uniform and smooth film formation. The UV-Vis properties were supported by computational chemistry, performed using density functional theory (DFT) for optimizing geometry and absorption of TT-Pc models. Sensitive and selective responses of 90% and 60% were obtained from **TT-Pc** OFET-based sensors upon exposure to 20 ppm of NO_2 and SO_2, respectively, under ambient conditions. One of the lowest limits of detection of ~165 ppb was achieved for both NO_2 and SO_2 using solution-processed **TT-Pc** sensor with natural, biodegradable dielectric biopolymer. The sensors showed excellent long-term environmental and operational stability with only a 7% reduction of the sensor's initial response (%) upon exposure to NO_2 and SO_2 over nine months of operation in air.

Keywords: Organic Field-Effect Transistors, Sustainable Gas Sensor, Biodegradable Dielectric, Room Temperature NO_2 And SO_2 Detection, Thienothiophene (TT), Phthalocyanine (Pc)

View Article Online
DOI: 10.1039/D4TC03208J

Introduction

Gas sensors are important requirement for air quality monitoring and food safety detection for toxic and pollutant gases such as nitrogen dioxide (NO_2), sulphur dioxide (SO_2), ammonia (NH_3), hydrogen sulfide (H_2S) and volatile organic compounds (VOC).[1-3] Conventional electronic noses (E-noses), which are generally made of resistor-type multi-sensor array based on metal oxides, require high operation temperature and power consumption and, hence, not suitable for flexible and portable sensors.[4] On the contrary, organic semiconductor FET-based gas sensors benefit from gate-modulated carrier concentration in the channel and, thus, exhibit superior merits in room-temperature operation and sensing response signal amplification.[5] OFET-based gas sensors detect gas species under certain environmental conditions by recording a change in device parameters, such as a change in OFET I_{DS} (at a constant V_{GS} and V_{DS}), mobility, threshold voltage, etc.[6] The employment of OFET platforms as gas sensors is an efficient method for selective gas identification and provides a fingerprint for gas recognition.[7] As a general rule, the sensing mechanism of OFET sensors is described by the charge distribution at the semiconductor/dielectric interface upon exposure to gas. Depending on the properties and morphology of the active layer, the gaseous analyte may induce charge trapping/detrapping and, hence, increase/decrease of the potential barrier between continuous grains, leading to a change in the source-drain current, threshold voltage and mobility.[8] Unfortunately, OFETs generally use synthetic polymer dielectrics processed from expensive and toxic organic solvents. Therefore, naturally occurring biopolymer dielectric materials deposited from low-cost, environmentally friendly solvents, such as water, are gaining attention in fabrication of electronic devices and circuits in environmentally friendly and sustainable way. It has been previously reported that natural gums such as gum arabic, almond gum and khaya gum are promising dielectric materials for sustainable fabrication of low voltage OFETs.[9,10] In particular, khaya gum, a natural substance of khaya senegalensis trees, with excellent dielectric (k value of 7), antimicrobial, non-toxicity, biodegradability, and water solubility properties offers great opportunity for sustainable fabrication of low power OFET-based gas sensors.

View Article Online
DOI: 10.1039/D4TC03208J

Phthalocyanines (Pcs), a member of tetraisoindole macrocyclic molecular material series, have been attracting great attention since the first day they were synthesized.[11] The interest covers various fields ranging from photodynamic therapy agents in cancer treatment, nonlinear optic materials,[12] photo-initiators for polymerization,[13,14] chemical sensors,[15-19] organic semiconductors,[20] memory devices,[21] and, recently, to energy-based materials. This is due to their interesting spectroscopic, photochemical, and photophysical properties as well as high thermal and optical stabilities.[22] Moreover, Pcs have a conjugated 18 π-electron system, affording strong absorption and emission capabilities in near infrared region (NIR). Additionally, their easy modification, and introduction of various central metals and axial ligands attached to the central metal help to adjust the photochemical properties of phthalocyanine molecules.[23] Metal phthalocyanines (MPcs) are identified as promising organic semiconductors as gas sensors due to their outstanding thermal and chemical stability, and chemical sensitivity toward different reactive gases, especially oxidizing gases, *via* manipulation of the metal core.[24-27] In particular, zinc phthalocyanine (ZnPc) has shown excellent electrical performance, stability, and sensing capability to detect various gaseous analytes, which make it a suitable material for applications in organic integrated circuits, sensors, and photovoltaics.[2,28] Another group of well-known organic semiconductors are thienothiophenes (TTs) for energy-based materials. TTs are the simplest fused thiophenes, composed of two annulated thiophene rings, having four isomers.[29-33] The most widely used TT isomer is thieno[3,2-*b*]thiophene, providing continuous conjugation through two fused thiophenes when integrated to small molecules and polymers.[34-39] TTs have extended π-conjugation, planar structure, intermolecular S---S interaction, and electron rich, flat, rigid, and good electron delocalized skeleton.[40-44] These properties make them highly suitable and desirable main building blocks for organic electronics such as OLED, OFET, organic solar cells (OSC), capacitors and sensors.[45-52]

In this work, design and synthesis of a first example of TT (thieno[3,2-*b*]thiophene) and Pc-based semiconductor, **TT-Pc**, composed of nonyl-substituted TT and ZnPc, are reported. The novel **TT-Pc** was clarified by spectroscopic and microscopic methods such as UV-Vis, scanning electron microscopy (SEM), and atomic force microscopy (AFM). **TT-Pc** was incorporated into a field-effect transistor device having khaya gum dielectric layer to detect hazardous NO_2 and SO_2 gas analytes, operating at low voltage with high responsivity and sensitivity at room temperature. This novel OFET-based gas sensor provides new opportunities for the scalable production of high-performance flexible sensing electronics.

View Article Online
DOI: 10.1039/D4TC03208J

Results and Discussion

Design and Synthesis

The monoketone (**2**) and TT (**3**) were synthesized following our previous reports.[53-56] The reaction of 3-bromothiophene (**1**) with *n*-butyllithium at -78 °C was followed by addition of elemental sulfur and then α-haloketone to produce **2** in 88% yield. Its ring closure reaction was conducted in the presence of polyphosphoric acid (PPA) in refluxing chlorobenzene to give **3** in 83% yield. The TT (**3**) was monostannylated using *n*-butyllithium at -78 °C, which was followed by addition of tributyltin chloride to give **4**. Its Stille coupling reaction with 4-iodophthalonitrile was performed using Pd(0) as a catalyst in dry DMF to construct **5** in yield of 61% to be used as a main ligand. Cyclotetramerization reaction of **5** was conducted in the presence of zinc acetate ($Zn(OAc)_2$) and 1,8-diazabicyclo[5.4.0]undec-7-ene (DBU) to give **TT-Pc** in 52% yield (Scheme 1).

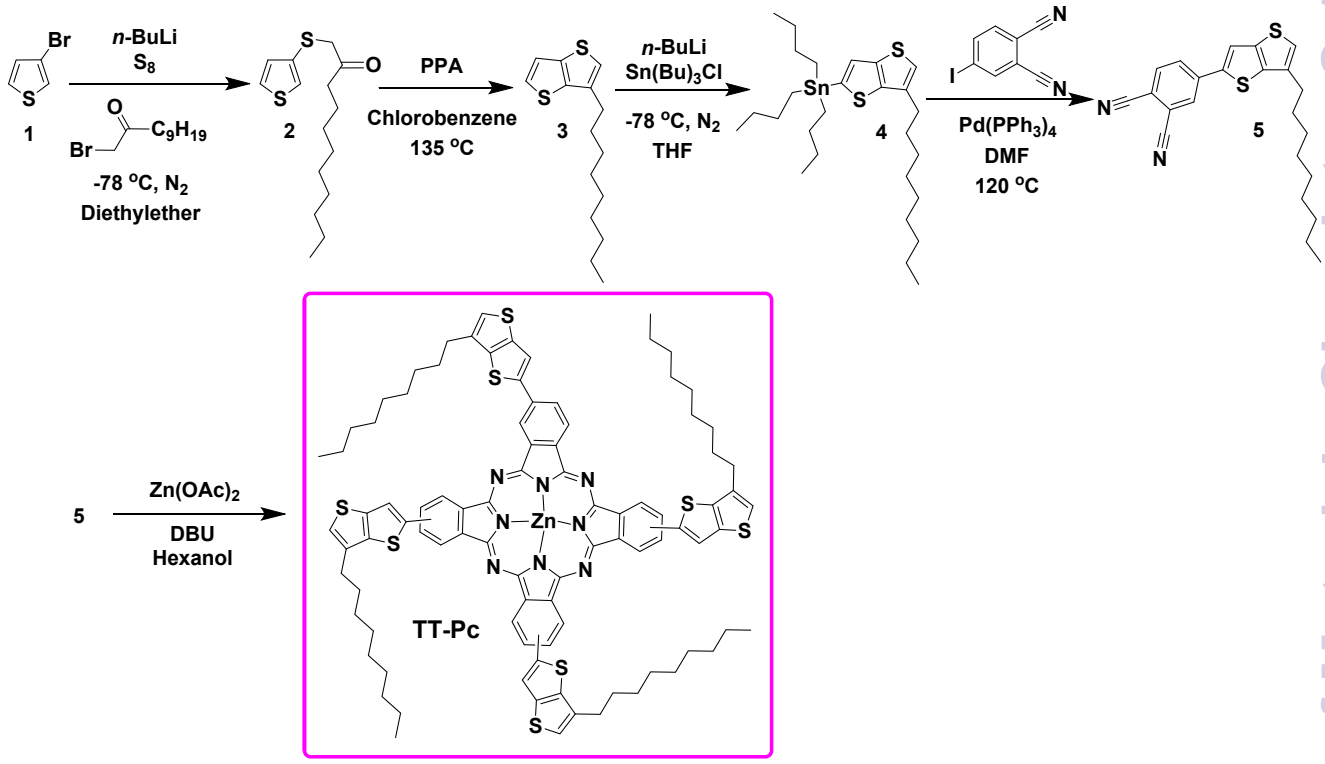

Scheme 1. Synthetic routes of the **TT-Pc**.

Photophysical Properties

Optical properties of **TT-Pc** were investigated by UV-Vis spectroscopy, which showed typical non-aggregated phthalocyanine B (Soret) and Q bands at 345 and 695 nm, respectively, in THF (Fig. 1). The optical band gap (E_{optic}) was calculated to be 1.69 eV from the onset threshold

View Article Online
DOI: 10.1039/D4TC03208J

wavelength of the absorption spectra at 732 nm. In addition to solution state properties, its film was deposited on the surface of ITO glass by spin-coating from a chloroform solution (2 mg. mL^{-1}) at ambient conditions. Solid-state UV-Vis maximums were determined to be 343 and 698 nm. A difference of ~3 nm between the maximum absorptions of its solution and film spectra suggested a low interaction in solution due to the length of the four alkyl chains (C_9H_{19}) on TT cores. Moreover, the shoulder intensity around 630 nm in solution increased in the film form, indicating a typical H-aggregate behavior of zinc-phthalocyanine on **TT-Pc** film. [57,58]

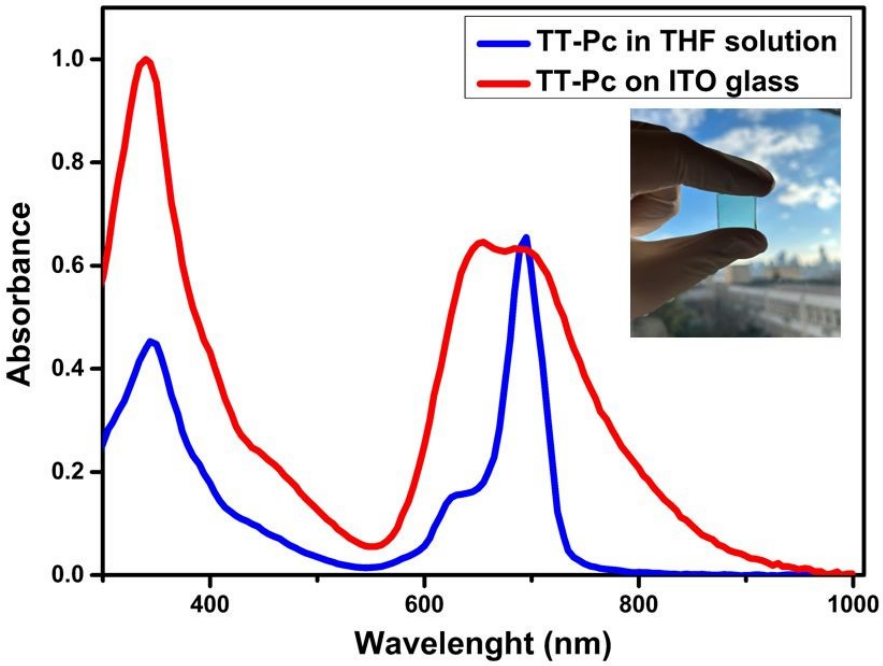

Fig. 1 UV-Vis spectroscopy of **TT-Pc** in THF solution and on ITO glass (inset: thin film of the **TT-Pc**).

Computational Study

Depending on the positions of the alkylated TT units around the Pc core, three possible conformations of **TT-Pc** models **(TT-Pc-1, TT-Pc-2**, and **TT-Pc-3)** were examined by computational chemistry. Different backbone geometries and their optimized structures were investigated at the level of B3LYP/6-31G (d, p) in the ground state.[59] Long alkyl chains on the TT moiety were replaced with methyl groups to simplify the calculation. Fig. 2 illustrates optimized top and side views of **TT-Pc-1, TT-Pc-2**, and **TT-Pc-3**. The molecular orbitals derived from HOMO and LUMO of Pc derivatives and their energy levels measured in eV are shown in Fig. 3. All structures displayed a similar band gap (E_g) around 2.00 eV with similar HOMO and LUMO energies around -4.90 and -2.87 eV, respectively.[13,24,25] While HOMO is

highly localized on the phthalocyanine core and partially on the TT unit, the phthalocyanine units contributed mainly to the LUMO. TD-DFT calculations were conducted to examine the electronic transition wavelengths and corresponding theoretical UV-Vis spectrums. Fig. S1 presents the absorption spectra of **TT-Pc** structures in THF simulated at CAM-B3LYP/6-31G (d, p). All the structures showed the strongest absorption at 663 nm, which is attributed to the Q band (Pc band), while the peaks observed in the region of the B band were in between 376-383 nm range. The theoretically predicted optical maximum values were found to be consistent with the corresponding experimental data.

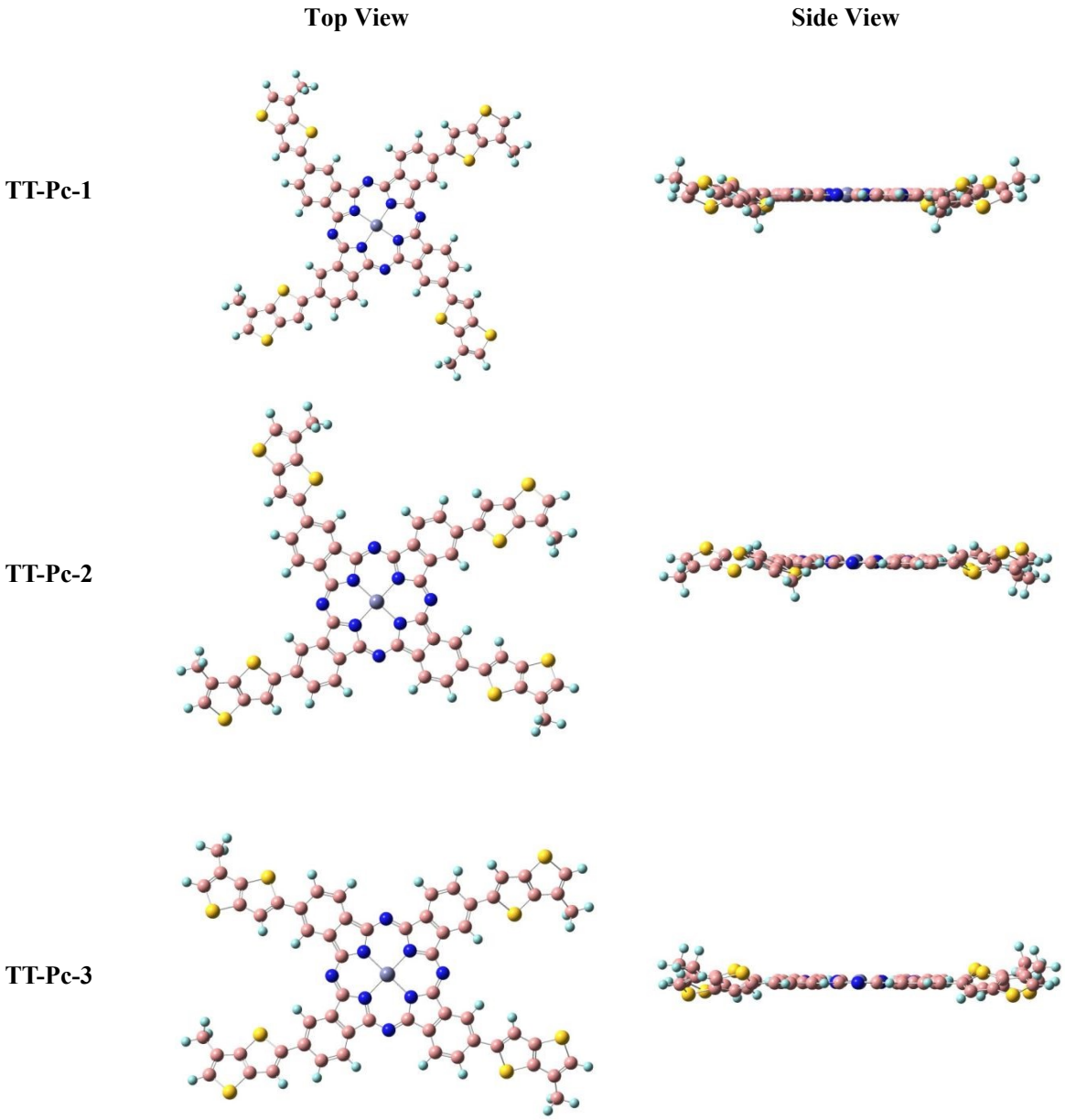

View Article Online
DOI: 10.1039/D4TC03208J

Fig. 2 Top and side view of **TT-Pc-1**, **TT-Pc-2**, and **TT-Pc-3** optimized at B3LYP/6-31G (d, p) level of theory.

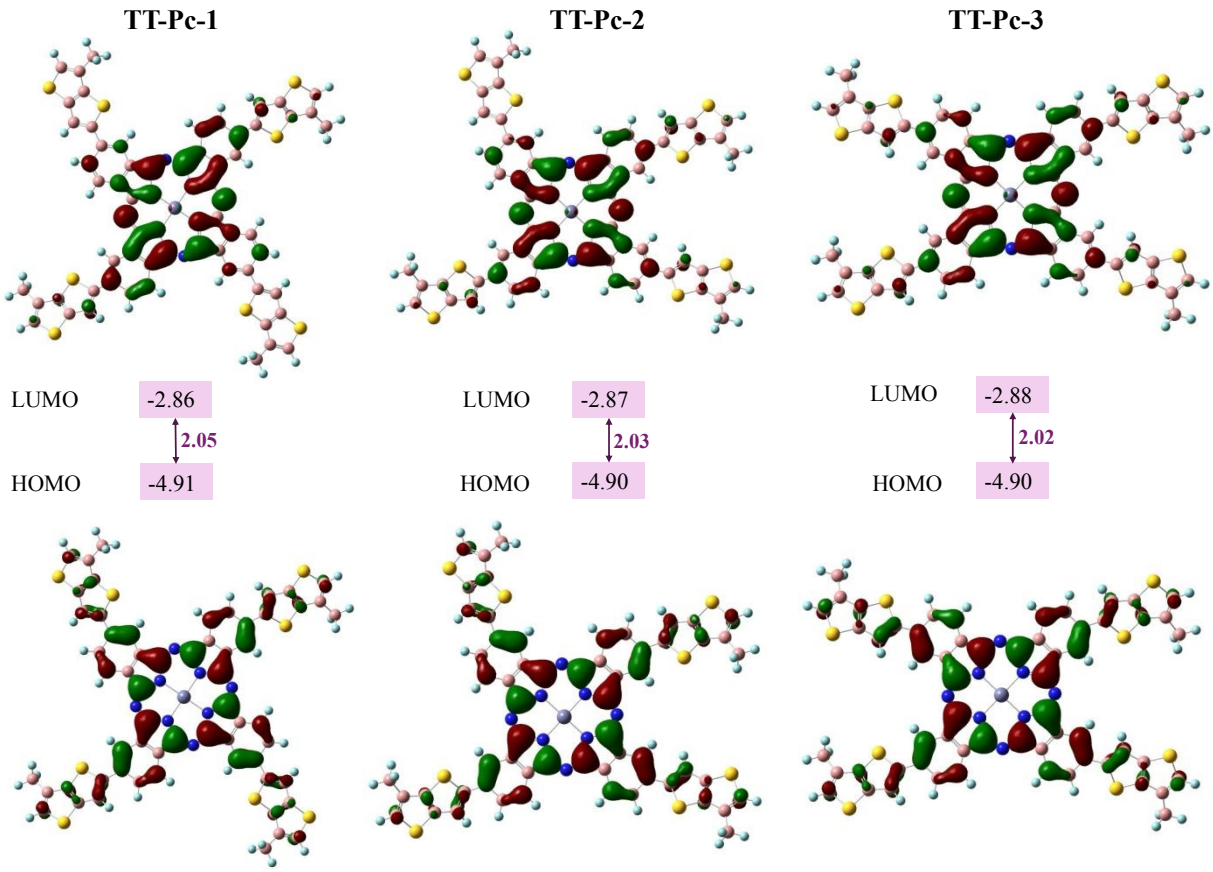

Fig. 3 HOMO and LUMO energy levels of optimized **TT-Pc** structures at B3LYP/6-31G (d, p) level of theory, and their energy gap values.

Surface Topography and Morphology

Surface morphology of **TT-Pc** film was investigated by scanning electron microscopy (SEM) and atomic force microscopy (AFM). SEM images indicated a quite smooth and clear surface of **TT-Pc** film with different scale bars of 2 and 200 μm (Fig. 4a and b). RMS roughness, obtained from the cross section of the AFM images, was determined to be 42 nm, demonstrating a relatively uniform and smooth surface morphology (Fig. 4c and d). It was illuminated with topographic visuals that **TT-Pc** is a very suitable material for film formation. Moreover, further surface property was investigated by contact angle (CA) measurement (Fig. 4e). Deposition of dH_2O sessile drop on the **TT-Pc** film showed a 122.3° CA, indicating a very high hydrophobic surface, which is higher than many Pc-based materials reported in the literature.[60,61]This is possibly due to the presence of long alkyl chains on already hydrophobic TT moieties.

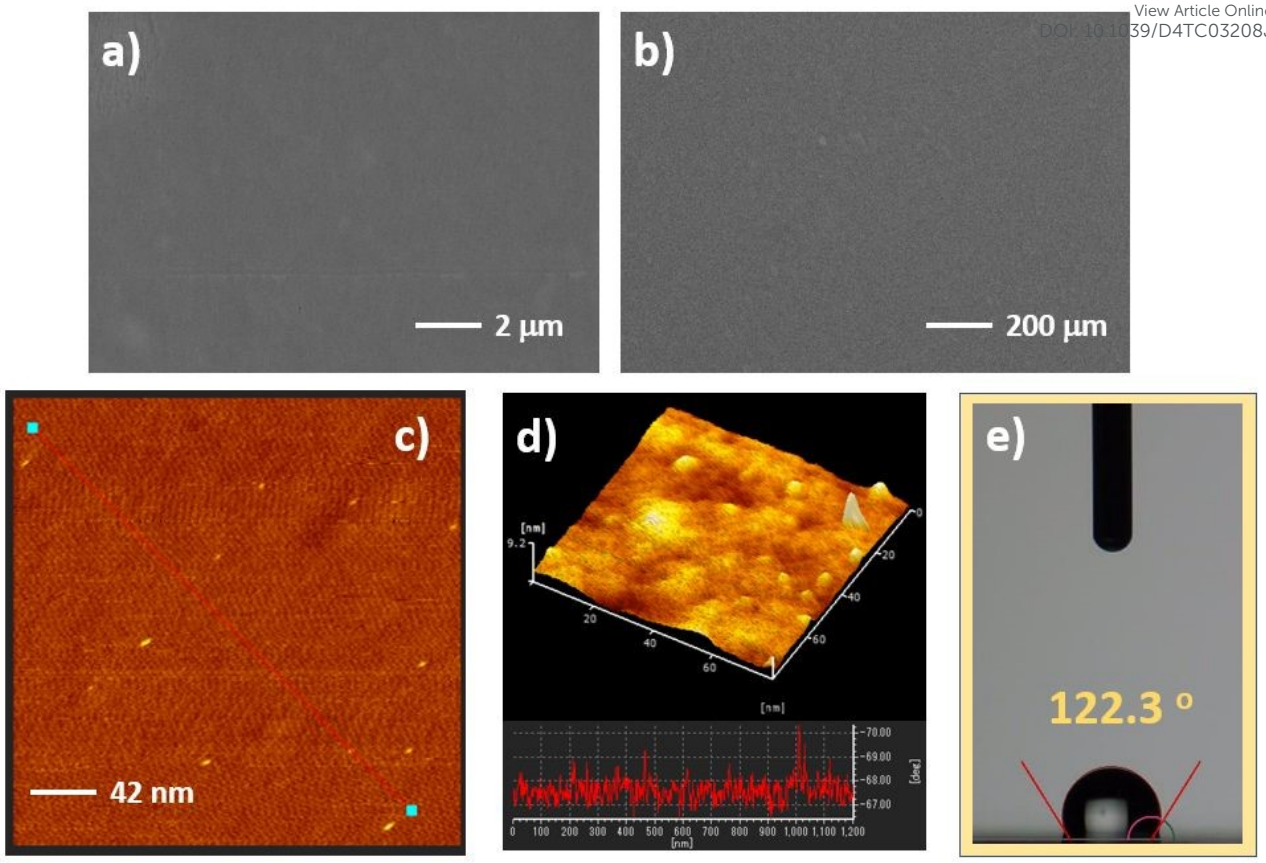

Fig. 4 (a) SEM image of **TT-Pc** film with scale bars of 2 µm and (b) 200 µm, (c) AFM images of **TT-Pc** film based on thickness of 42 nm. (d) 3D AFM surface topographic image and cross section analyses of **TT-Pc** film. (e) Contact angle image of the **TT-Pc** film using water droplet.

OFET Application and Gas Sensing Performance

The performance of **TT-Pc** as an active material in low voltage OFETs and sensing layer in room temperature gas sensors was evaluated. Bottom-gate, top-contact OFET devices (Fig. 5a) using khaya gum dielectric layer were used as sensing platforms to detect different concentrations of nitrogen dioxide (NO_2) and sulphur dioxide (SO_2) gases. Naturally occurring and biodegradable khaya gum (KG) was used as a high-k ($k \approx 7$)[62] gate dielectric layer to realize sustainable manufacturing of low-power, low-waste 'green' sensors.[63] The KG used in this work was collected from exudates of khaya senegalensis trees growing in Senegal (Fig. 5b). It is a natural polysaccharide known for its biodegradability, non-toxicity, water solubility, great dielectric properties[64] and anti-inflammatory features.[65] The purification process of KG powder (Fig. 5c) is described elsewhere.[62]A 2.5 wt. % solution of KG in deionized water was spun at 3500 rpm for 2 min onto pattered aluminum gate electrodes. The KG layer was annealed at 100 °C for 30 minutes at ambient conditions, giving a thickness of ~200 nm. The **TT-Pc** was, then,

View Article Online
DOI: 10.1039/D4TC03208J

spin-coated as the semiconductor channel from a 1wt % 1,2-dichlorobenzene solution and annealed at 90 °C for 2 hours. Finally, source and drain gold electrodes were evaporated throw shadow masks, creating OFETs with channel length (L) and width (W) of 30 μm and 1000 μm, respectively.

Each substrate consisted of 20 OFETs with identical channel dimensions. Each transistor was characterized under ambient conditions (air with 45% relative humidity) using an Agilent E5270B measurement mainframe with Karl Suss PH100 micromanipulator probes. All the OFET parameters were calculated in the saturation regime using the standard metal-oxide semiconductor field-effect transistor (MOSFET) equation;[66]

$$I_{DS,sat} = \frac{W}{2L}\mu C_i(V_{GS} - V_{th})^2$$

where $I_{DS,sat}$ is the drain current in the saturation regime, W is the channel width, L is the channel length, μ represents the field-effect carrier mobility, Ci is the areal capacitance of the dielectric layer and V_{GS} and Vth are the gate voltage and threshold voltage, respectively. As previously reported, the Ci value for khaya gum is calculated to be ~ 130 nF/cm^2 at 1 kHz.[62]

The transfer and leakage current characteristics of the OFETs using **TT-Pc** as the active material are presented in Fig. 5d and Fig. S2, respectively. The transistors were operated in the accumulation mode and distinctively displayed p-type field-effect behavior under a gate voltage (V_{GS}) of -3 V. As observed from the transfer curve, devices exhibit a good pinch-off with clear distinctive linear and saturation regimes and negligible hysteresis between the forward and reverse sweeps. The leakage current through khaya gum dielectric layer is more than two orders of magnitude lower than the "on" current (I_{DS}) at -3 V. The figures-of-merit of 20 characterized OFETs are collated in Table 1. The average hole mobility (~ 0.025 cm^2/Vs) of the OFETs in this work are comparable to and in some cases higher than those in the literature using solution processed ZnPc. The mobility values of MPcs depend on the central metal atom, gate dielectric, and the deposition techniques.[67] In addition, these low voltages operating OFETs showed significantly smaller subthreshold swing (at least one order of magnitude) than similar devices using MPcs.[68-70]Moreover, compared to the previously reported solution-processed OFETs using khaya gum as dielectric layer,[62] these **TT-Pc** transistors showed a notably smaller (two folds) subthreshold swing. Nevertheless, compared to their counterparts, the herein fabricated OFETs, applying solution-processed **TT-Pc**, yielded superior field-effect performance, particularly at very low voltages, using a naturally occurring dielectric layer.

View Article Online
DOI: 10.1039/D4TC03208J

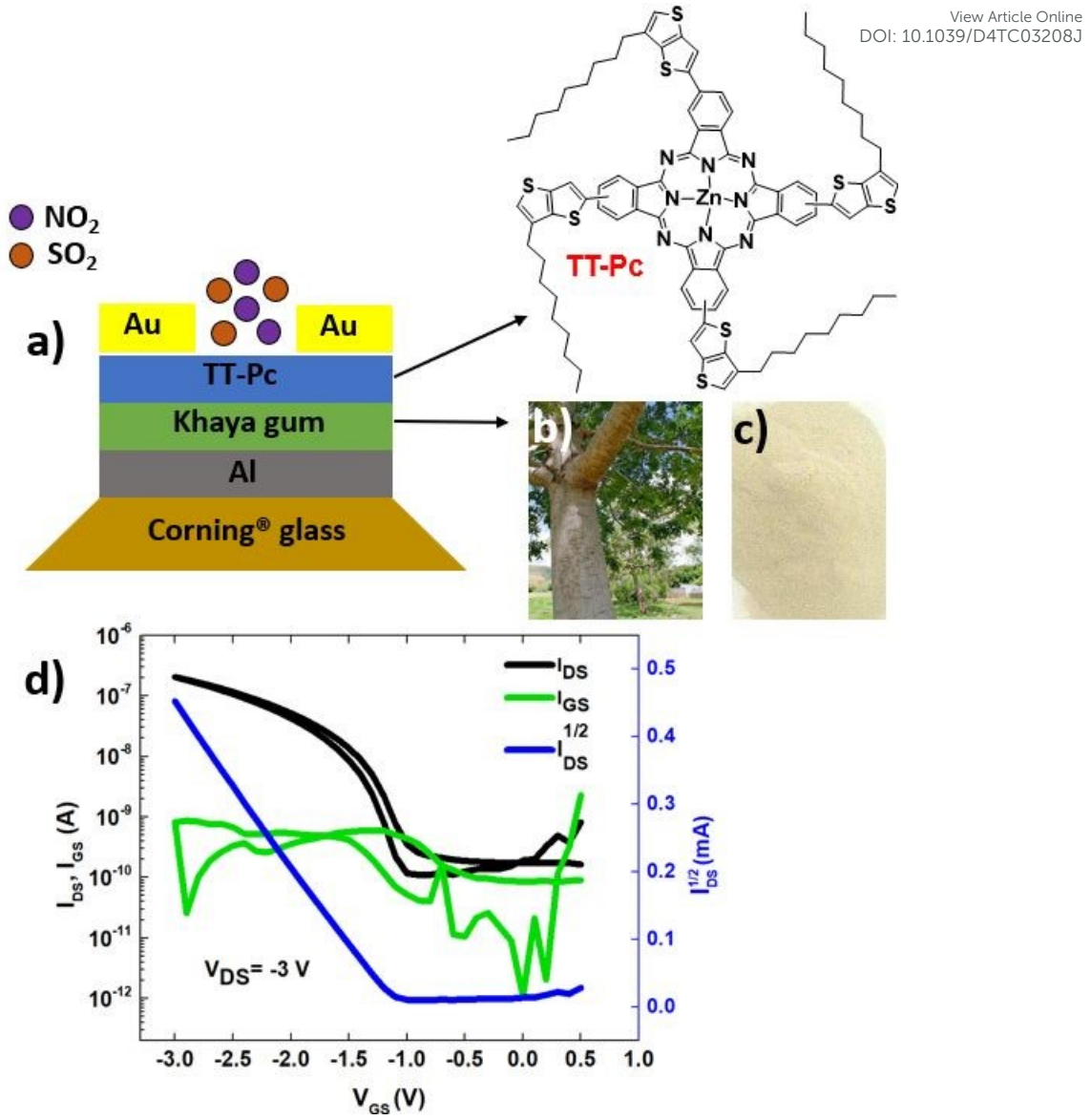

Fig. 5 (a) Configuration of the fabricated bottom-gate, top-contact OFET platform as a gas sensor, (b) khaya senegalensis tree, (c) khaya gum powder post-purification and (d) transfer characteristics of **TT-Pc** OFETs.

Table 1. Figures-of-merit of **TT-Pc** OFETs.

Average hole mobility (μ_{sat}) cm²/Vs	**Threshold Voltage V_{th} (V)**	**I_{on}/I_{off}**	**Subthreshold Swing (SS) mV/dec**
2.5 x 10^{-2} ± 0.5	-1.1 ± 0.1	>10^3	230 ± 20

The characterized **TT-Pc** OFETs were subsequently evaluated as gas sensing platforms upon exposure to different concentrations of two redox gases, i.e. nitrogen dioxide (NO_2) and sulphur

View Article Online
DOI: 10.1039/D4TC03208J

dioxide (SO_2), under ambient conditions (23 °C and 45% relative humidity). In this context, we report a highly sensitive room temperature operated NO_2 and SO_2 gas sensors based on low-voltage, and **TT-Pc**-based OFETs, using naturally occurring khaya gum as the dielectric material. Different concentrations of NO_2 and SO_2 were obtained by feeding a mixture of dry air and the selected gaseous analytes in appropriate volumes through a mass flow controller. Prior to introducing the adjusted concentrations to the sensors, a baseline was recorded exposure of the devices to dry air only. The OFET-based sensors were then exposed to sequential concentrations, from 20 ppm down to 100 ppb, of each gas separately under ambient conditions.

The transfer curves of OFETs in dry air and after exposure to each specific concentration of NO_2 and SO_2 are plotted in Figure 6. Both sets of I_{DS} *vs* V_{GS} curves manifested a directly proportional increase in IDS as the concentration of the target gases increased. NO_2 is an oxidizing gas that is believed to increase the conductivity of p-type OFETs during exposure.[28] NO_2 diffuses into the **TT-Pc** active layer and displaces absorbed species such as oxygen, creating charge carriers (holes) in the semiconducting layer, thereby, increasing the I_{DS} of OFET at a constant bias and inducing positive shifts in Vth (Fig. 6a). On the other hand, where the target gas is the nonoxidizing SO_2, the binding of the gas molecule to both the electron donating thienothiophene and the zinc center of ZnPc of the active layer may alter conduction through the entire semiconductor layer. Similarly, an increase in I_{DS} and positive shift in Vth of OFETs is recorded upon exposure to different concentrations of SO_2 (Fig. 6b). In agreement with the literature,[71] thiophene monomer donates to or accepts electrons from specific analytes, for instance, SO_2 and NH_3, respectively, which results in positive I_{DS} change for SO_2. Nonetheless, it is highly speculated that both target gas molecules can bind to the zinc metal at the center of the phthalocyanine in **TT-Pc** and cause a change in the overall conduction of the active channel.[28]

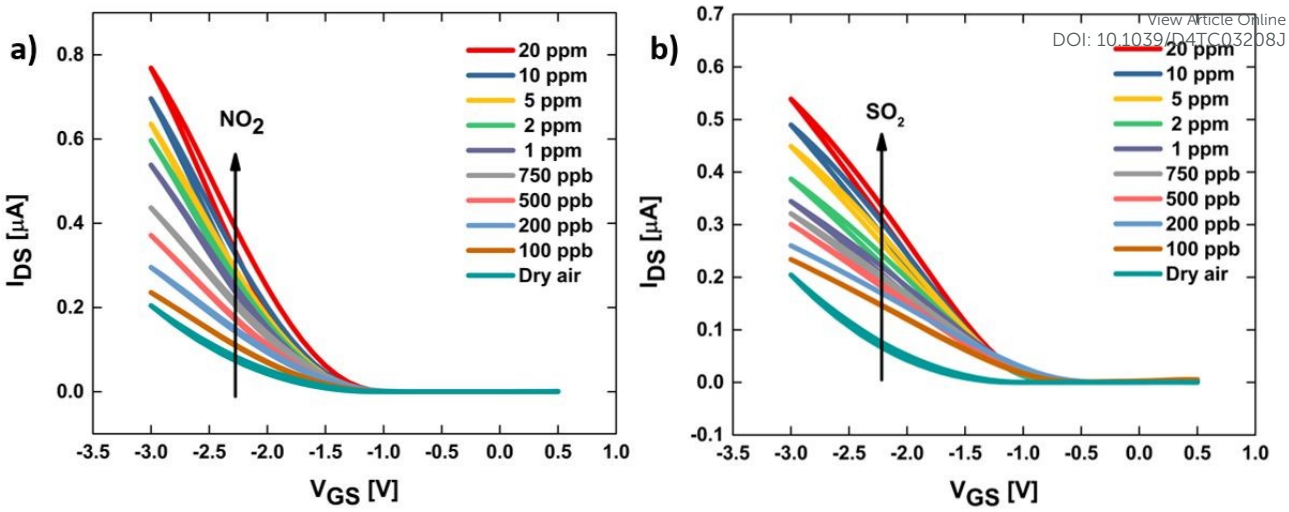

Fig. 6 Transfer characteristics of **TT-Pc** OFET platforms in response to dry air and various concentrations of (a) NO_2 and (b) SO_2 at room temperature.

The room temperature transient response of sensors upon exposure to sequential concentrations of NO_2 and SO_2 from 20 ppm down to 100 ppb under ambient conditions was investigated (Fig. 7). The exposure and recovery times were found to be 2 and 5 minutes, respectively.

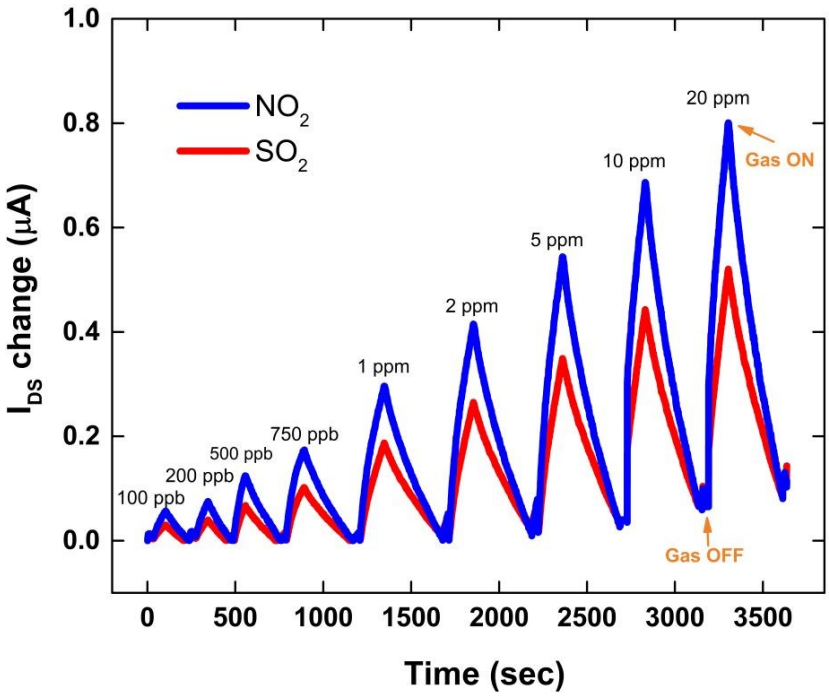

Fig. 7 Room temperature transient sensor response upon exposure to sequential concentrations of NO_2 and SO_2 from 20 ppm down to 100 ppb.

View Article Online
DOI: 10.1039/D4TC03208J

In agreement with the transfer curves plotted in Figure 8, a progressively significant increase in the transient responses of the **TT-Pc** OFET-based sensors was recorded upon exposure to sequential concentrations of NO_2 and SO_2 from 20 ppm down to 100 ppb. The sensor showed good response and recovery to different concentrations of both gases. However, higher I_{DS} change (about 25%) was observed for NO_2, compared to SO_2. This could be attributed to the stronger interaction of oxidizing NO_2 and higher sensitivity of **TT-Pc** active layer to NO_2. At 20 ppm, a substantial 0.8 μA and 0.5 μA increase in I_{DS} was recorded for NO_2 and SO_2, respectively. It is worth mentioning that, as the concentration of the gaseous analytes increased, a moderate drift from the original baseline was observed for both gases only at higher concentrations. Although MPcs demonstrate a very high sensitivity towards oxidizing gases like NO_2, they suffer from a prolonged recovery. Such a slow recovery is due to strong chemisorption of the gas molecules onto the sensor surface.[72] However, in this work, the sensors consistently recovered to the baseline within 5 minutes assigned time, showing reversibility with negligible drift for lower gas concentrations (< 2 ppm). This was ascribed to the adopted top-contact configuration of the OFET platform, which only exposes the channel area (3×10^{-4} cm^2) to the analyte and the remaining semiconductor layer under the top contacts is kept intact. The thinner the semiconductor layer and the smaller the active area of the OFET sensor exposed to the gas are, the faster the response and the recovery time will become.

As a key merit of gas sensors, the response of the OFET platforms upon exposure to the target gases was calculated using the equation;

$$Relative\ Response\ (\%) = \left(\frac{I_{Gas} - I_0}{I_0}\right) \times 100$$

where I_{Gas} is the I_{DS} value after exposure to the selected gas and I_0 is the baseline value, immediately before exposure. Moreover, the evaluation of responses from the baseline (dry air) is required. The calibration curve obtained by plotting the response (R) for each gaseous analyte *vs* its concentrations is shown in Figure 8a.

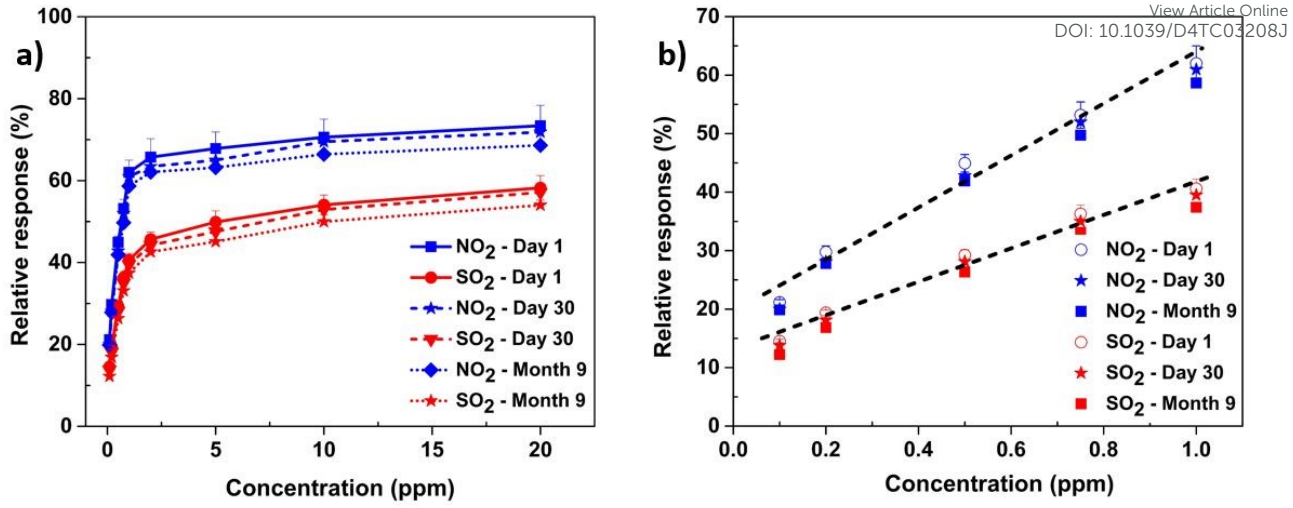

Fig. 8. (a) The NO_2 and SO_2 sensors calibration curves and (b) the linear fit to response at lower concentration regime for both NO_2 and SO_2.

A significant and never previously reported response of 90% and 60% were obtained for the **TT-Pc** OFETs upon exposure to 20 ppm of NO_2 and SO_2 (using air as carrier gas), respectively, under ambient conditions. Moreover, a distinguishable differentiation between the sensor responses to NO_2 and SO_2 is observed, which makes these low-voltage **TT-Pc** OFETs a promising gas sensor for room temperature operation with high sensitivity.

Long-term stability of the sensor's performance was evaluated over one month and nine months of operation in air. The experimental results in Figure 8a showed only a 5-7% reduction of the sensor's initial response (%) upon exposure to NO_2 and SO_2 of the same concentration range. The linearity of the calibration curve for sensor's responses to both gases obtained on day 1, day 30 and month 9 (Figure 8b), was determined by an adequate regression analysis of the data of the lower concentrations. Based on the linear fit of the calibration curve, the theoretical lower limit of detection (LOD) is extrapolated. The LOD is defined as the lowest concentration of a gas corresponding to the smallest signal that can be detected with reasonable certainty, but not necessarily quantified as an exact value.[8] It is often denoted as (3 × N/S), where N is the noise of the baseline (the sensors response in the absence of gas) and S is the sensitivity of the sensor. From the linear fit in Figure 8b, the LOD for both NO_2 and SO_2 was estimated to be ~165 ppb, which is one of the lowest limits of detection reported for solution-processed, low-voltage OFET-based sensors using natural, biodegradable dielectric biopolymers.[72-73] As collated in Table 2, although a lower value of LOD for NO_2 was reported using ZnO nanowire-FET, the sensor was fabricated at a very high temperature, operated at high voltage and detected only one type of gas. Similarly, despite lower limit of detection, graphene-based sensors not

only were fabricated using high-temperature and timely techniques, but also operated at high voltage with single-element sensing capability. On the other hand, OFET sensors using DPP-based polymers that showed a much lower limit of detection for SO_2, were operating at high voltage and did not show any response against other gases, for example NO_2. Moreover, current examples of nanosheet-based materials have also been used as sensors for NO_2, but these materials require high operation temperature and power consumption.[74-82]

Herein, the reported **TT-Pc** sensors show excellent sensitivity, low LOD, good response time and reversibility, low drift, long-term environmental and operational stability, and good sensing response to oxidizing NO_2 and non-oxidizing SO_2 gases. The sensors were only tested under ambient conditions, without varying moisture content of gas mixture to avoid probable degradation of the sensing material upon repetitive exposure. This approach allowed evaluation of sensor's long-term operational stability in detection of NO_2 and SO_2. Using natural biopolymer khaya gum enables sustainable fabrication of low-cost, low-power gas sensors for cost-effective, fast, and reliable domestic, industrial and ecosystem air quality monitoring.

Table 2. Summary and comparison of the morphology and charge transport characteristics of various OFET-based gas sensors in the literature and the present work.

Sensing Material	Deposition	Dielectric	Operating Voltage (V)	Detected Gas	LOD (ppb)	Ref.
SWCNT	Hot filament chemical vapor deposition (HF-CVD)	SiO_2	-4	NO_2	560	74
SWCNT	Aerosol jet printed	AlO_x	-1.5	NO_2	69	75
ZnO-NW	Printing and calcination at 200-700°	SiO_2	80	NO_2	0.05	76
Mg-porphyrin modified graphene	CVD	SiO_2	40	NO_2	52	77

View Article Online
DOI: 10.1039/D4TC03208J

Pentacene	Thermal evaporation	Polystyrene on SiO_2	-60	NO_2	100	78
P3HT	Spin-cast	PMMA/poly-TPD blend (solution-cast)	-40	NO_2	242.6	79
DPP-based polymers	Spin-cast	SiO_2	-80	SO_2	0.24	80
MoS_2 Nanosheets	Thermal evaporation	-	6	NO_2	62.5	81
$ZnIn_2S_4$ Nanosheets	Thermal evaporation	-	-0.6	NO_2	130	82
TT-Pc	Spin-cast	Natural biopolymer (Khaya gum) processed from water	< -3	NO_2 and SO_2	165	This work

Conclusion

In this work, a novel, sustainable strategy for low power, low-cost OFET-based NO_2 and SO_2 sensors with high responsivity and sensitivity has been realized using **TT-Pc** as an active layer. Naturally occurring khaya gum processed from water is used as the dielectric layer to promote sustainable and environmentally friendly fabrication of the reported gas sensors. **TT-Pc**, composed of nonyl substituted thienothiophene (TT) and Zn phthalocyanine (ZnPc), was clarified by SEM, AFM and contact angle measurements, indicating an excellent film formation and a superior hydrophobic surface with 122.3° water droplet. **TT-Pc** was successfully fabricated for a low voltage OFET device using biodegradable and water soluble khaya gum (KG) dielectric at room temperature. A remarkable response of 90% and 60% were achieved for the **TT-Pc** OFETs upon exposure to 20 ppm of NO_2 and SO_2, respectively, under ambient conditions. The obtained LOD of ~165 ppb for both NO_2 and SO_2 is one of the lowest recorded for solution-processed polymer sensors using biodegradable dielectric materials. Moreover, these low-voltage OFET-based sensors yielded great long-term stability with less than 7% reduction of the sensor's initial response (%) upon exposure to NO_2 and SO_2 over nine months

View Article Online
DOI: 10.1039/D4TC03208J

of operation in air. In brief, the present study introduced a sustainable approach towards fabrication of novel OFET sensor for detection toxic and pollutant NO_2 and SO_2 gases based on a **TT-Pc** structure that can satisfy the rigorous requirements for highly sensitive and stable gas sensors for practical applications with possibility of reducing the adverse environmental impacts.

Experimental Details

Materials

All the reagents were purchased from Aldrich and Acros and used without further purification. All the solvents, used in the syntheses, were technical grade and freshly distilled prior to use. The solvents, used in spectroscopic measurements, were spectroscopic grade. Flash chromatography was performed with ≤ 0.063 μm Silica Gel. ^{1}H and ^{13}C NMR spectra were recorded on a Varian 500 and 126 MHz, respectively, spectrometer. Proton and carbon chemical shifts are reported in parts per million downfield from tetramethylsilane, TMS.

Synthesis

Synthesis of 1-(thiophen-3-ylthio)undecan-2-one (2). To a solution of 3-bromothiophene **1** (2.0 g, 12.25 mmol) in dry diethyl ether (40 mL), a solution of *n*-butyllithium in hexane (5.4 mL, 13.50 mmol, 2.5 M) was added dropwise at -78 °C, under nitrogen atmosphere. After the reaction was stirred for 1 h, elemental sulfur (S_8) (0.41 g, 12.85 mmol) was added, and the mixture was further stirred for 45 min. Then, 1-bromoundecan-2-one (3.66 g, 14,70 mmol) was introduced portion wise. Stirring was continued overnight, and the reaction was quenched with water. The solution was extracted with dichloromethane, and the organic layer was washed with Na_2CO_3 solution (10%) and water. The organic layer was dried over Na_2SO_4, filtered and the solvent was evaporated under reduced pressure. The crude product was purified by flash column chromatography eluting with a mixture of *n*-hexane: CH_2Cl_2 (5:1) to give the title compound **2** as a yellowish powder (3.07 g, 88%). ^{1}H NMR (500 MHz, $CDCl_3$) δ 7.33 (dd, J = 5.0, 3.0 Hz, 1H), 7.22 (dd, J = 3.0, 1.3 Hz, 1H), 7.03 (dd, J = 5.0, 1.3 Hz, 1H), 3.58 (s, 2H), 2.57 (t, J = 7.4 Hz, 2H), 1.62-1.58 (m, 2H), 1.33-1.22 (m, 12H), 0.89 (t, J = 7.0 Hz, 3H). ^{13}C NMR (126 MHz, $CDCl_3$) δ 205.77, 130.04, 129.59, 126.53, 124.98, 45.00, 40.68, 31.85, 30.92, 29.39, 29.34, 29.24, 29.11, 23.82, 22.65, 14.10.

Synthesis of 3-nonylthieno[3,2-*b*]thiophene (3). To a solution of polyphosphoric acid (PPA) (3.58 g, 35.10 mmol) in chlorobenzene (10 mL) at 135 °C was added **2** (1.0 g, 3.51

mmol), dissolved in chlorobenzene (5 mL), dropwise. The reaction was stirred at this temperature for 8 h, after which the mixture was extracted with CH_2Cl_2, $NaHCO_3$ solution (10%) and water. The organic layer was dried over Na_2SO_4, filtered and the solvent was evaporated under reduced pressure. The residue was purified by column chromatography eluting with a mixture of *n*-hexane to obtain the title compound **3** as a yellowish oil (0.78 g, 83%). ^{1}H NMR (500 MHz, $CDCl_3$) δ 7.38 (d, J = 6.3 Hz, 1H), 7.27 (d, J = 5.2 Hz, 1H), 7.02 (s, 1H), 2.76 (t, J = 7.7 Hz, 2H), 1.82-1.75 (m, 2H), 1.42-1.29 (m, 12H), 0.92 (t, J = 6.2 Hz, 3H). ^{13}C NMR (126 MHz, $CDCl_3$) δ 139.96, 138.70, 134.89, 126.54, 121.70, 119.90, 31.91, 29.98, 29.55, 29.42, 29.39, 29.33, 28.63, 22.70, 14.13.

Synthesis of tributyl(6-nonylthieno[3,2-*b*]thiophen-2-yl)stannane (4). To a solution of **3** (600 mg, 2.25 mmol) in 40 mL THF, a solution of *n*-butyllithium in hexane (1.80 mL, 2.82 mmol, 1.6 M) was added dropwise at -78 °C under nitrogen atmosphere. The solution was stirred at -78 °C for 1 h and 1.0 M solution of tributyltin chloride (4.23 mL, 4.23 mmol) in THF was added in one portion. The solution was warmed to room temperature and stirred overnight. The reaction was quenched with water. The organic layer was extracted with twice brine and water. The organic layer was dried over anhydrous Na_2SO_4. The organic layer was evaporated under reduced pressure and the product **4** was used for next step without further purification.

Synthesis of 4-(6-nonylthieno[3,2-*b*]thiophen-2-yl)phthalonitrile (5). To a solution of 4-iodophthalonitrile (200 mg, 0.79 mmol) and **4** (670 mg, 1.20 mmol), dissolved in DMF (20 mL) and degassed for 20 min under nitrogen, was added $Pd(PPh_3)_4$ (91 mg, 0.079 mmol) at room temperature in dark. The reaction mixture was heated and stirred at 120 °C for 48 h. The reaction flask was then cooled to room temperature and the mixture was poured into a concentrated KF solution. The resulting suspension was extracted several times with CH_2Cl_2. Afterward, the combined organic layers were washed with distilled water and dried over anhydrous sodium sulfate. The solvent was removed under reduced pressure and the crude product was purified by column chromatography eluting with *n*-hexane:CH_2Cl_2 (1:1) to obtain light yellow pure compound **5** (187 mg, 61%). ^{1}H NMR (500 MHz, $CDCl_3$) δ 7.94 (s, 1H), 7.85 (d, J = 8.3 Hz, 1H), 7.74 (d, J = 9.0 Hz, 1H), 7.61 (d, J = 1.1 Hz, 1H), 7.12 (d, J = 0.6 Hz, 1H), 2.73 (t, J = 7.7 Hz, 2H), 1.76 (dt, J = 14.6, 7.1 Hz, 2H), 1.39-1.27 (m, 12H), 0.89 (t, J = 6.5 Hz, 3H). ^{13}C NMR (126 MHz, $CDCl_3$) δ 141.39, 140.06, 139.92, 139.78, 135.22, 133.96, 129.50, 128.82, 124.69, 119.39, 116.58, 115.50, 115.24, 112.94, 31.89, 29.79, 29.53, 29.40, 29.35, 29.31, 28.57, 22.69, 14.15. MALDI-TOF-MS (m/z): [M] calcd. for $C_{23}H_{24}N_2S_2$, 392.58; found, 391.382.

Synthesis of TT-Pc. A mixture of **(5)** (190 mg, 0.48 mmol) and anhydrous zinc acetate (29.6 mg, 0.16 mmol) in dry hexanol (1.5 mL) in a Schlenk tube was sonicated for 5 min. Subsequently, the reaction mixture was stirred for 20 min under argon atmosphere and heated to 120 °C. At this temperature DBU (50.0 µL) was added and the tube was sealed. The reaction mixture was stirred at 160 °C for 6 h. It was then cooled to room temperature and the mixture was precipitated in methanol and centrifuged. The crude product was purified by column chromatography eluting initially with CH_2Cl_2: THF (20:1) and then THF. The solid product was washed with hot methanol for several times to obtain **TT-Pc** as a dark green powder (98 mg, 52%). ^{1}H NMR (600 MHz, THF-d_8) δ 11.18-10.55 (m, 10H), 9.92 (m, 8H), 9.14 (d, J = 16.8 Hz, 2H), 4.90-4.74 (m, 7H), 4.35-4.26 (m, 7H), 3.80 (8H), 3.49-3.25 (m, 45H), 2.83 (m, 9H). ^{13}C NMR (151 MHz, THF-d_8) δ 153.01, 152.89, 147.19, 147.11, 147.09, 145.37, 145.29, 142.40, 142.20, 141.14, 141.10, 140.60, 140.56, 140.52, 140.49, 139.52, 139.44, 137.55, 137.46, 137.39, 137.02, 136.45, 136.10, 126.85, 126.75, 126.48, 126.39, 125.85, 125.82, 123.74, 123.60, 123.44, 123.41, 123.01, 119.67, 119.44, 119.28, 118.23, 118.16, 118.08, 117.99, 33.20, 33.18, 32.88, 31.09, 30.96, 30.88, 30.85, 30.75, 30.67, 30.62, 30.14, 30.01, 23.87, 14.76, 14.75, 13.41, 13.35, 13.31. MALDI-TOF-MS (m/z): [M] calcd. for $C_{92}H_{96}N_8S_8Zn$, 1635.70; found, 1635.103.

Conflict of interest

There are no conflicts to declare.

Acknowledgments

The authors thank ITU (Istanbul Technical University), TDA-2022-43696, TDA-2024-45680, TGA-2023-44077 and TGA-2023-45124 numbered ITU BAP Projects, 122Z568 numbered TUBITAK 1001 Project and Unsped Global Lojistik, Turkey, for financial supports. The authors would like to thank Prof. Abdou Karim Diallo at the Université Gaston Berger for providing the Khaya gum.

References

1. W. Huang, J. Sinha, M. -L. Yeh, J. F. M. Hardigree, R. LeCover, K. Besar, A. M. Rule, P. N. Breysse, H. E. Katz, *Adv. Funct.Mater.* 2013, **23,** 4094-4104.
2. H. Gou, G. Wang, Y. Tong, Q. Tang, Y. Liu, *Org. Electron*. 2016, **30,** 158-164.
3. A. Kumar, R. Meunier-Prest, M. Bouvet, *Sensors* 2020, **20,** 4700.
4. Z. Song, Q. Tang, Y. Tong, Y. Liu, *IEEE Electron Device Lett.* 2017, **38,** 11, 1586-1589.
5. C. Zhang, P. Chen, W. Hu, *Chem. Soc. Rev.* 2015, **44,** 2087–2107.

6. S. Han, Z. Yang, Z. Li, X. Zhuang, D. Akinwande, J. Yu, *ACS Appl. Mater. Interfaces* 2018, **10,** 44, 38280-38286.
7. L. Torsi, A. Dodabalapur, L. Sabbatini, P. G. Zambonin, *Sens. Actuators B, Chem.* 2000, **67,** 3, 312-316.
8. L. Torsi, M. Magliulo, K. Manoli, G. Palazzo, *Chem. Soc. Rev.* 2013, **42,** 8612-8628.
9. M. Seck, N. Mohammadian, A. K. Diallo, S. Faraji, M. Saadi, M. Erouel, E. H. B. Ly, K. Khirouni, L. A. Majewski, *Synth. Met.* 2020, **267,** 116447.
10. M. Seck, N. Mohammadian, A. K. Diallo, S. Faraji, M. Saadi, M. Erouel, E. H. B. Ly, K. Khirouni, L. A. Majewski, *Org. Electron.* 2020, **83,** 105.
11. A. B. P. Lever, C. C. Leznoff, VCH: New York, 1989-1996.
12. M. Louzada, J. Britton, T. Nyokong, S. Khene, *J. Phys. Chem. A* 2017, **121,** (38), 7165-7175.
13. L. Breloy, O. Yavuz, I. Yilmaz, Y. Yagci, D. L. Versace, *Polym. Chem.* 2021, **12***,* (30), 4291-4316.
14. L. Breloy, V. Brezová, A. Blacha-Grzechnik, M. Presset, M. S. Yildirim, I. Yilmaz, Y. Yagci, D. L. Versace, *Macromolecules* 2020, **53,** 112–124.
15. O. Yavuz, Y. Alcay, K. Kaya, M. Sezen, S. K. Atasen, M. S. Yildirim, Y. Ozkilic, N. S. Tuzun, I. Yilmaz, *Inorg. Chem.* 2019, **58** (1), 909-923.
16. O. Yavuz, M. Sezen, Y. Alcay, M. S. Yildirim, K. Kaya, Y. Ozkilic, N. Ş. Tuzun, I. Yilmaz, *Sens. Actuators B Chem.* 2021, **329,** 129002.
17. O. Yavuz, M. Sezen, Y. Alcay, M. S. Yildirim, H. Aribuga, E. Ozdemir, U. Ertugral, Y. Ozkilic, N. S. Tuzun, I. Yilmaz, *Spectrochim. Acta A Mol. Biomol. Spectrosc.* 2023, **284,** 121484.
18. D. Cetin, O. Yavuz, Y. Alcay, M. S. Yildirim, M. Kaplan, H. Aribuga, E. Ozdemir, U. Ertugral, I. Yilmaz, *Spectrochim. Acta A Mol. Biomol. Spectrosc.* 2023, **297,** 122725.
19. M. S. Yildirim, Y. Alcay, O. Yavuz, S. K. Atasen, Z. Mermer, H. Aribuga, I. Yilmaz, *Anal Chim. Acta* 2022, **1198,** 339531.
20. G. De La Torre, C. G. Claessens, T. Torres, *Chem. Commun.* 2007, **20,** 2000-2015.
21. B. Das, M. Samanta, P. Sarkar, U. K. Ghorai, A. Mallik, K. K. Chattopadhyay, *Adv Electron Mater***.** 2021, **7** (4), 2001079
22. G. Lu, X. Kong, P. Ma, K. Wang, Y. Y. Chen, J. Jiang, *ACS Appl. Mater. Interfaces* 2016, **8,** 9, 6174-6182.
23. T. Nyokong, *Coord. Chem. Rev.* 2007, **251** (13-14), 1707-1722.

24. M. Chaabene, B. Gassoumi, P. Mignon, R. B. Chaabane, A. R. Allouche, *J. Mol. Graph.* 2019, **88,** 174-182.
25. A. G. Martynov, J. Mack, K. A. May, T. Nyokong, Y. G. Gorbunova, A. Y. Tsivadze, *ACS Omega* 2019, **4,** 7265-7284.
26. F. I. Bohrer, A. Sharoni, C. Colesniuc, J. Park, I. K. Schuller, A. C. Kummel, W. C. Trogler, *J. Am. Chem. Soc*. 2007, **129,** 17, 5640-5646.
27. S. Ji, H. Wang, T. Wang, D. A. Yan, *Adv. Mater.* 2013, **25,** 1755-1760.
28. F. D'Souza, E. Maligaspe, K. Ohkubo, M. E. Zandler, N. K. Subbaiyan, S. Fukuzumi, *J. Am. Chem. Soc.* 2009, **131,** 25, 8787-8797.
29. R. Isci, E. Tekin, K. Kaya, S. P. Mucur, S. F. Gorkem, T. Ozturk, *J. Mater. Chem. C* 2020, **8,** 7908-7915.
30. R. Isci, E. Tekin, S. P. Mucur, T. Ozturk, *ChemistrySelect* 2020, **5,** 13091-13098.
31. M. E. Cinar, T. Ozturk, *Chem. Rev.* 2015, **115** (9), 3036-3140.
32. G. Turkoglu, M. E. Cinar, T. Ozturk, *Eur. J. Org. Chem.* 2017, **31,** 4552–4561.
33. R. Isci, M. Unal, G. Kucukcakir, N. A. Gurbuz, S. F. Gorkem, T. Ozturk, *J. Phys. Chem. B* 2021, **125,** 13309-13319.
34. R. Isci, A. R. Varzeghani, K. Kaya, B. Sütay, E. Tekin, T. Ozturk, *ACS Sustainable Chem. Eng.* 2022, **10,** 4, 1605-1615.
35. R. Isci, E. Baysak, G. Kesan, B. Minofar, M. S. Eroglu, O. Duygulu, S. F. Gorkem, T. Ozturk, *Nanoscale* 2022, **14,** 16602-16610.
36. B. Amna, R. Isci, H. M. Siddiqi, L. A. Majewski, S. Faraji, T. Ozturk, *J. Mater. Chem. C* 2022, **10** (21) (2022) 8254-8265.
37. R. Isci, D. Gunturkun, A. S. Yalin, T. Ozturk, *J. Polym. Sci.* 2021, **59,** 117-123.
38. R. Isci, L. Wan, S. Topal, D. Gunturkun, A. J. Campbell, T. Ozturk, *J. Mater. Chem. C* 2022**, 10** (29) 10719-10727.
39. R. Isci, E. Gencosman, Y. Yagci, and T. Ozturk, *J. Photochem. Photobiol. A* 2024, **449,** 115427.
40. H. Bronstein, Z. Chen, R. S. Ashraf, W. Zhang, J. Du, J. R. Durrant, P. S. Tuladhar, K. Song, S. E. Watkins, Y. Geerts, M. M. Wienk, R. A. J. Janssen, T. Anthopoulos, H. Sirringhaus, M. Heeney, I. McCulloch, *J. Am. Chem. Soc.* 2011, **133** (10), 3272-3275.
41. F. Turksoy, J. D. Wallis, U. Tunca, T. Ozturk, *Tetrahedron* 2003, **59** (41) 8107-8116.
42. E. Ertas, T. Ozturk, *Tetrahedron Lett.* 2004, **45** (17), 3405-3407.

43. G. Yildiz, Z. Aydogmus, M. E. Cinar, F. Senkal, T. Ozturk, *Talanta* 2017, **173,** 1-8
44. G. M'. Baye, A. S. Klymchenko, D. A. Yushchenko, V. V. Shvadchak, T. Ozturk, Y. Mély, G. Duportail, *Photochem. Photobiol. Sci.* 2007, **6** (1), 71-76.
45. T. Ozturk, C. R. Rice, J. D. Wallis, *Mater. Chem.* 1995, **5,** 1553-1556.
46. E. Akman, S. Akin, T. Ozturk, B. Gulveren, S. Sonmezoglu, *Solar Energy* 2020, **202,** 227-237.
47. N. Saygili, R. J. Brown, P. Day, R. Hoelzl, P. Kathirgamanathan, E. R. Mageean, T.; Oztuk, M. Pilkington, M. M. B. Qayyum, S. S. Turner, L. Vorgerrw, J. D. Wallis, *Tetrahedron* 2001, **57** (23), 5015–5026.
48. R. Isci, T. Balkan, S. Tafazoli, B. Sütay, M. S. Eroglu, T. Ozturk, *ACS Appl. Energy Mater.* 2022, **5,** 13284-13292.
49. S. E. Ozturk, R. Isci, S. Faraji, B. Sütay, L. A. Majewski, T. Ozturk, *Eur. Polym. J.* 2023, **191,** 112028.
50. D. Gunturkun, R. Isci, B. Sütay, L. A. Majewski, S. Faraji, T. Ozturk, *Eur. Polym. J.* 2022, **170,** 111167.
51. R. Isci, T. Ozturk, *Turk. J. Chem.* 2023, **47,** 5, 1239-1248.
52. A. Suerkan, R. Isci, T. Ozturk, Y. Yagci, *Mol. Syst. Des. Eng.* 2023, **8,** 10, 1319-1326.
53. R. Isci, M. Unal, T. Yesil, A. Ekici, B. Sütay, C. Zafer, T. Ozturk, *Front. Mater.* 2023, **10,** 1125462.
54. D. Gunturkun, R. Isci, S. Faraji, B. Sütay, L. A. Majewski, T. Ozturk, *J. Mater. Chem. C* 2023, **11,** 38, 13129-13141.
55. R. Isci, T. Ozturk, *Beilstein J. Org. Chem.* 2023, **19,** 1849-1857.
56. R. Isci, K. B. Donmez, Y. Karatepe, T. Ozturk, *ACS Appl. Energy Mater.* 2024, **7,** 4, 1488-1494.
57. M. Bayda, F. Dumoulin, G. L. Hug, J. Koput, R. Gorniaka, A. Wojcik, *Dalton Trans*., 2017, **46,** 1914-1926.
58. S. Doria, A. Lapini, M. D. Donato, R. Righini, N. Azzaroli, A. Iagatti, J. R. Caram, T. S. Sinclair, L. Cupellini, S. Jurinovich, B. Mennucci, G. Zanotti, A. M. Paoletti, G. Pennesi P. Fogg, *Phys. Chem. Chem. Phys.,* 2018, **20,** 22331-22341.
59. M. J. Frisch, G. W. Trucks, H. B. Schlegel, G. E. Scuseria, M. A. Robb, J. R. Cheeseman, G. Scalmani, V. Barone, G. A. Petersson, H. Nakatsuji, X. Li, M. Caricato, A. V. Marenich, J. Bloino, B. G. Janesko, R. Gomperts, B. Mennucci, H. P. Hratchian, J. V. Ortiz, A. F. Izmaylov, J. L. Sonnenberg, D. Williams-Young, F. Ding, F. Lipparini, F. Egidi, J. Goings,

B. Peng, A. Petrone, T. Henderson, D. Ranasinghe, V. G. Zakrzewski, J. Gao, N. Rega, G. Zheng, W. Liang, M. Hada, M. Ehara, K. Toyota, R. Fukuda, J. Hasegawa, M. Ishida, T. Nakajima, Y. Honda, O. Kitao, H. Nakai, T. Vreven, K. Throssell, J. A. Montgomery, Jr., J. E. Peralta, F. Ogliaro, M. J. Bearpark, J. J. Heyd, E. N. Brothers, K. N. Kudin, V. N. Staroverov, T. A. Keith, R. Kobayashi, J. Normand, K. Raghavachari, A. P. Rendell, J. C. Burant, S. S. Iyengar, J. Tomasi, M. Cossi, J. M. Millam, M. Klene, C. Adamo, R. Cammi, J. W. Ochterski, R. L. Martin, K. Morokuma, O. Farkas, J. B. Foresman, and D. J. Fox, Gaussian, Inc., Wallingford CT, 2016.

60. J. B. Brito, D. J. C. Gomes, V. D. Justina, A. M. F. Lima, C. A. Olivati, J. R. Silva, N. C. de Souza, *J. Colloid Interface Sci.* 2012, **367** (1), 467-471.
61. A. Dekshinamoorthy, P. P. Samal, S. Krishnamurty, P. K. Khatri, S. L. Jain, A. Ray, S. Vijayaraghavan, *Langmuir* 2023, **39** (48), 17295-17307.
62. A. Tall, S. Faraji, A. K. Diallo, N. Mohammadian, M. Erouel, M. Seck, M. Saadi, K. Khirouni, L. A. Majewski, *J Mater Sci: Mater. Electron* 2022, **33,** 15283-15295.
63. M. Seck, N. Mohammadian, A. K. Diallo, S. Faraji, M. Saadi, M. Erouel, E. H. B. Ly, K. Khirouni, L. A. Majewski, *Org. Electron.* 2020, **83,** 105.
64. A. Tall, A. K. Diallo, M. Erouel, M. Seck, L. Chouiref, M. Saadi, M. A. Wederni, E. H. B. Ly, A. Diallo, N. Bouguila, D. Kobor, K. Khirouni, *J Sol-Gel Sci Technol.* 2022, **104,** 401-411.
65. M. M. Zhou, W. Y. Zhang, R. J. Li, C. Guo, S. S. Wei, X. M. Tian, J. Luo, L. Y. Kong, *Phytomedicine* 2018, **42***,* 152-163.
66. H. Liu, A. T. Neal, P. D. Ye, *ACS Nano* 2012*,* **6** (10) 8563-8569.
67. L. Li, Q. Tang, H. Li, W. Hu, X. Yang, Z. Shuai, Y. Liu, D. Zhu, *Pure Appl. Chem.* 2008, **80,** 11, 2231-2240.
68. A. Sharma, M. Zahedi, M. Durmuş, T. Basova, A. Ray, V. Ahsen, N. Chaure, *J. Appl. Phys.* 2010, **107***,* 114503.
69. G. Chaidogiannos, F. Petraki, N. Glezos, S. Kennou, S. Nešpůrek, *Appl. Phys. A: Mater. Sci. Process.* 2009, **96,** 763-767.
70. O. A. Melville, B. H. Lessard, and T. P. Bender, *ACS Appl. Mater. Interfaces* 2015, **7,** 24, 13105-13118.
71. H. Sajid, T. Mahmood and K. Ayub, *J Mol. Model*. 2017, **23,** 295.
72. P. Kumar, V. N. Mishra, R. Prakash, *IEEE Sens. J.* 2023, **23** (12), 12544-12551,
73. S. Tyagi, M. Chaudhary, A. K. Ambedkar, K. Sharma, Y. K. Gautama B. P. Singh, *Sens. Diagn.* 2022, **1,** 106-129.

74. S. Forel, L. Sacco, A. Castan, I. Florea, C. S. Cojocaru, *Nanoscale Adv.* 2021, **3,** 1582-1587.
75. X. Wang, M. Wei, X. Li, S. Shao, Y. Ren, W. Xu, M. Li, W. Liu, X. Liu, J. Zhao, *ACS Appl. Mater. Interfaces,* 2020, **12,** 51797-51807.
76. S. Oh, J.-I. Cho, B. H. Lee, S. Seo, J.-H. Lee, H. Choo, K. Heo, S. Y. Lee, J.-H. Park, *Sci. Adv.* 2021, **7,** eabg9450.
77. T. Ikuta, T. Tamaki, H. Masai, R. Nakanishi, K. Endo, J. Terao, K. Maehashi, *Nanoscale Adv.* 2021, **3,** 5793-5800.
78. M. Mirza, J. Wang, L. Wang, J. He, C. Jiang, *Org. Electron.* 2015, **24,** 96-100.
79. Z. Yang, X. Zhuang, S. Han, J. Yu, *Mater. Lett.* 2019, **236,** 285-288.
80. Y. Kang, D. H. Kwak, J. E. Kwon, B.-G. Kim, W. H. Lee, *ACS Appl. Mater. Interfaces* 2021, **13,** 31910-31918.
81. K. Zhao, X. Chang, J. Zhang, F. Yuan, X. Liu, *ACS Sens.* 2024, **9,** 388-397.
82. C. Wang, X. Chang, X. Liu, J. Zhang, *J. Phys. Chem. Lett.* 2024, **15,** 5875-5882.

View Article Online
DOI: 10.1039/D4TC03208J

Data Availability Statement

The authors confirm that the data supporting the findings of this study are available within the article and its Supporting material. Raw data that support the findings of this study are available from the corresponding author, upon reasonable request.